SPECTROSCOPIC INVESTIGATION OF PROTEINS

by

Benjamin Kabagambe

B.S. in Chemistry, LaRoche College, 2004

Submitted to the Graduate Faculty of

College of Arts and Sciences in partial fulfillment

of the requirements for the degree of

Master of Science in Chemistry

University of Pittsburgh

2007

UNIVERSITY OF PITTSBURGH

FACULTY OF ARTS AND SCIENCES

This thesis was presented

by

Benjamin Kabagambe

It was defended on

October 12, 2007

and approved by

Stephen Weber, Professor, Department of Chemistry

Adrian Michael, Professor, Department of Chemistry

Thesis Advisor: Sanford A. Asher, Distinguished Professor, Department of Chemistry

SPECTROSCOPIC INVESTIGATION OF PROTEINS

Benjamin Kabagambe, M.S.

University of Pittsburgh, 2007

Apomyoglobin is obtained from pure myoglobin by extracting out the heme group. Using UV-visible spectrometry we are able to monitor complete removal of heme group. This extraction initiates the disruption of myoglobin's tertiary conformation. Apomyoglobin consists of 8 α-helices labeled A through H. These helices unfold when the protein is subjected to pH decrease. It is more compact at about pH 7 and unfolds as we change to more acidic environment. At about pH 2 we have A, G, H core with the rest of the helices unfolded. At pH values slightly lower than 2, A, G and H helices are also unfolded. When the protein is not denatured, the refolding process is done by changing the pH towards neutral. At pH 2, G and H helices refold and at pH 4 A-helix refolds as well. We have been able to label A-helix with protons and the rest of the protein with deuterium using H_2O and D_2O respectively. We have then used temperature change to initiate the unfolding of protonated A-helix. When dissolved in D_2O, the protonated A-helix at elevated temperatures, exchanges its N-H protons to N-D deuterons. Temperatures were elevated from 0° C to 80°C and changes in Am III peak intensities were observed using UV resonance Raman spectroscopy. These peak changes were quantified and used to calculate the number of N-H bonds present between 0° C and 80°C. The number of N-H bonds decreased with increase in temperature indicating the unfolding of A-helix.

TABLE OF CONTENTS

LIST OF TABLES

LIST OF FIGURES

ACKNOWLEDGEMENTS.

1.0 INTRODUCTION TO PROTEIN FOLDING.

Protein folding is one of the most fundamental problems of the 21st century. Studies of protein folding provide a better understanding of molecular processes underlying disease which in turn helps in better drug design. These studies are complicated by the fact that the system presents innumerable degrees of freedom. The interaction of the peptide geometry determines the conformation of the peptide. The thermodynamic factors that drive high entropy (unfolded state) or low entropy (native state) of the system have to be understood in order to better understand the folding process. In the following sections we describe some of these factors and how they affect the folding process.

1.1 ELECTROSTATIC INTERACTIONS

Electrostatic interactions play a significant role in protein folding. These are interactions between ionizable side chains e.g. carboxylate and ammonium ions on aspartic and lysine side chains, respectively. These interactions form ionic bonds-salt bridges. However, most charged amino acids lie on the protein surface and it's rare to find interior ionic bonding. Although rare, the ionic bonds can be important to protein structure especially in peptide structures where the positively charged N and the negatively charged O are a few angstroms away from each other.

1.2   HYDROGEN BONDING

Hydrogen bonds result from interactions between atoms bearing partial negative charge and partially positively charged hydrogen atoms. The 3-D structures of proteins are heavily dependent on a variety of networks of H-bonds. The H-bond interactions could be between atoms on two different amino acid sidechains. It could also be between amino acid sidechain and solvent molecules at the protein surface. Studies have shown that the native state secondary structure is a result of hydrogen bonds between backbone carbonyl (C=O) and amide (N-H).[1] These intramolecular hydrogen bonds are also responsible for formation and stabilization of α-helix. Furthermore, hydrogen bonding between two adjacent β-strands leads to β-sheet structure.

1.3   HYDROPHOBIC INTERACTIONS

One major force driving proper protein folding is hydrophobic interactions. These interactions form an interior hydrophobic core in which non polar sidechains closely associate and minimize their interaction with polar solvent molecules. All non polar chains are found inside the backbone where they are not exposed to the polar solvent. When they come to the surface they are usually involved in other extensive hydrophobic interactions.

The concept behind hydrophobic collapse is explained by Frank and Evans frozen "Iceberg model."[2-4] When dissolved in water, the non-soluble solutes are surrounded by water molecules which gain an ordered form and are considered to have low entropy. In hydrophobic collapse the hydrophobic parts of the protein come together expelling the water molecules with more entropy. As a result the system gains free energy which is referred to as liberation energy

thus, making the collapse a spontaneous process. The collapse results in isolation of non-polar solutes thus, resulting in a compact state which has less degrees of freedom. This enhances fast folding.

1.4   DISULFIDE BRIDGES

Disulfide bridges are usually formed by two sulfylhydryl (-SH) groups of cysteine residues. They are usually found in tertiary globules where their purpose is basically to provide extra stability to the tertiary structure.

1.5   VAN DER WAALS INTERACTION

The Van der Waals interactions are the weakest of all interactions mentioned above. They result from the existence of an electron cloud around the atom. The shifts of the electron cloud around the nucleus yields a temporary electric dipole on an atom. The transient dipole in one atom induces a complementary dipole in another atom, provided the two are very close to each other. These forces are weak but their large number makes them an important player in determining protein structures. Most atoms in proteins are packed very close to each other and therefore they are involved in forming these Van der Waals interactions. These Van der Waals interactions along with H-bonding and others are biologically recognized in the antibody-antigen recognition where the "lock and key" fit of two molecules.

1.6   METHODOLOGY FOR FOLDING STUDIES

The driving forces behind protein folding have led researchers to develop all kinds of models to help them have a better understanding of the process.[5-12] The "New View"[1] model for example, holds that, folding is an ensemble in which the peptide chain has large conformational entropy at the beginning of folding and then hydrophobic collapse and folding process leads to a spectacular decrease in conformational space for the system facilitating fast folding.[1] Folding continues in a funnel-like energy landscape until the native state is achieved.

In recent years many different experimental techniques have been developed to directly probe the protein energy landscape. The most prominent techniques in place are X-ray crystallography[13], NMR [14], Fluorescence[15], Infrared Spectroscopy (IR)[16], Circular Dichroism[17], Mass Spectrometry[18], and UV Resonance Raman spectroscopy (UVRRS).

The most detailed information about three dimension structures of proteins is given by X-ray crystallography, but it requires well defined crystal structures, however, the crystal structure may not provide information relevant to human needs. Furthermore, it prevents the study of the dynamic behavior of proteins. In theory NMR can provide detailed information on local and global protein structure, however, the technique suffers from spectral congestion and broadening.[19] In order to perform NMR experiments, there is need for high peptide/protein concentrations and this can induce aggregation in large proteins like myoglobin. In addition there is a time scale that limits kinetic resolutions to milliseconds time regime.[1] These problems are usually overcome by using expensive and laborious isotopic labeling and combined multidimensional pulsed NMR spectrometers.

Circular dichroism provides information on conformation of secondary structure, however, there is strong interference from $\pi \to \pi^*$ transition of aromatic residues which can confound quantification of secondary structure content.[20, 21]

UVRRS offers the best novel approach of determining equilibrium conformation and peptide folding dynamics. It gives better information content, and provides relative ease of handling and sample preparation as will be seen in the next sub-section. It also has the potential to examine experimental time scales from picoseconds to hours.[22]

1.6.1   UV RESONANCE RAMAN SPECTROSCOPY

Ultraviolet resonance Raman (UVRR) spectroscopy has typically been used to study small isolated secondary structures providing detailed information and basic steps required for studying biomolecular structure and function.[23, 24] Chi et al. developed a procedure for determining the percentage of α-helix and β-sheet composition in dilute solutions. They used the 206.5 nm light to excite within the $\pi \to \pi^*$ region and acquired resonance enhanced spectra.[25] There are amide bands in resonance enhanced spectra that provide a convenient way of characterizing the protein backbone conformation. These bands include amide I, II, III and $C_\alpha H$ vibrations which result from secondary structure. These bands are used to characterize the protein structure and dynamics, for example an increase in $C_\alpha H$ band intensity is an indicator of unfolding.

UVRRS based T-jump spectrometer is used to perform time-resolved measurements. Lednev et al.[26] used this spectrometer to do kinetic measurements of AP peptides with temporal resolution of about 3 ns and were able to see the early steps of protein unfolding. Asher et al. have recently followed the AP peptide melting profile and found that it melts from a helical

structure to a PPII helix conformation.[1] This paper has offered support to the recent theoretical studies that have suggested that small peptides in their unfolded state[27, 28] have more PPII helix conformation.[29, 30]

In later chapters of this document, UVRRS is used to study the unfolding of apomyoglobin. Using 204 nm light, we excited the amide regions of the protein. We then decoupled some motions in the amide backbone by changing the protein environment from H_2O and D_2O as illustrated in chapter 3. UVRRS methodology provides hope to improve our understanding of protein folding in the future.

2.0 RAMAN EFFECT: CLASSICAL AND QUANTUM MECHANICAL TREATMENT

2.1 INTRODUCTION

The Raman Effect is a light scattering phenomenon in which the incident and scattered light possess different frequencies as seen in figure 1. Unlike in absorption processes, in scattering processes, the energy of the incident photon doesn't have to be equal to the difference between two discrete energy levels of the system. Experiments have shown however, that as the energy of the incident photon gets closer to an electronic transition energy associated with the transition from ground to excited state of a system, the scattering intensity is enhanced.[31] This enhancement increases rapidly as the incident photon energy approaches an electronic transition energy and this is what is termed resonance scattering. Resonance scattering differs significantly from normal scattering as will be discussed in detail in this chapter.
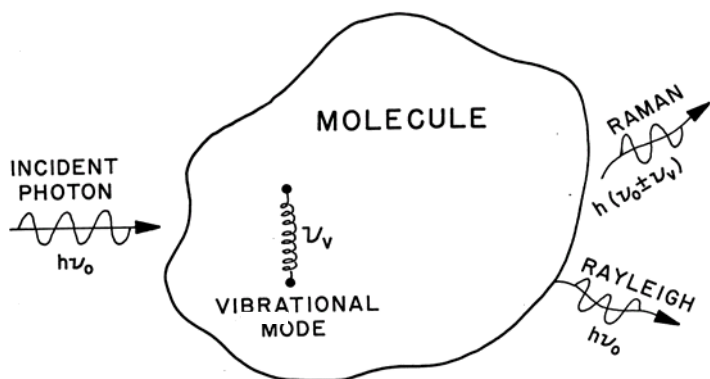
Figure 1 Illustration of scattering of an incident electromagnetic radiation from a laser source. Asher S. A. [32]

In both the classical and quantum mechanical treatments, the scattered radiation originates from electric and magnetic multipole moments induced in a molecule by electromagnetic fields of the incident radiation. The most significant contribution is from an oscillating electric dipole. The dipole moment induced in a molecule by an electric field of incident radiation of frequency ω_1, oriented at an angle θ with the axis of the dipole, gives intensity I shown in equation 1.

$$I = k'_\omega \omega_s^4 p_0^2 \sin^2 \theta \tag{1}$$

$$k'_\omega = \frac{1}{32\pi^2 \varepsilon_0 c_0^3} \tag{2}$$

The p_0 term is the amplitude of the induced electric dipole with frequency ω_s. Classical and quantum mechanical treatments have been done to find how ω_s and p_0 relate to properties of the scattering molecule and the incident electromagnetic radiation of frequency ω_1.

2.2   CLASSICAL TREATMENT

The objective of this section is to calculate the frequency dependent linear induced dipole vector $p^{(1)}$ using its relationship with electric field vector of the incident radiation E.

$$p^{(1)} = \alpha \cdot E \tag{3}$$

The polarizability tensor α of a molecule is a function of nuclear coordinates. In this treatment we will assume a space-fixed molecule in its equilibrium configuration with the nuclei vibrating about the equilibrium position. The polarizability varies with the vibrations of the molecule in away expressed in the following equation.

$$\alpha_{\rho\sigma} = (\alpha_{\rho\sigma})_0 + \sum_k (\frac{\partial \alpha_{\rho\sigma}}{\partial Q_k})_0 Q_k + \frac{1}{2} \sum_{k,l} (\frac{\partial^2 \alpha_{\rho\sigma}}{\partial Q_k \partial Q_l})_0 Q_k Q_l \cdots \tag{4}$$

Where $(\alpha_{\rho\sigma})_0$ represents the value of $\alpha_{\rho\sigma}$ at equilibrium configuration and Q_k and Q_l are normal coordinates of the molecular vibrational frequencies ω_k and ω_l respectively. The above equation is a Taylor series summation of all normal modes. We will ignore all modes with Q higher than the first order. We may therefore write this as:

$$(\alpha_{\rho\sigma})_k = (\alpha_{\rho\sigma})_0 + (\alpha'_{\rho\sigma})_k Q_k \tag{5}$$

Where

$$(\alpha'_{\rho\sigma})_k = (\frac{\partial \alpha_{\rho\sigma}}{\partial Q_k})_0 \tag{6}$$

Now assuming mechanical harmonicity, the time dependent coordinate Q_k is given by the equation;

$$Q_k = Q_{k_0} \cos(\omega_k t + \delta_k) \tag{7}$$

9

Q_{k_0}, δ_k are normal coordinate amplitude and phase factor respectively. To find obtain the time dependent $\alpha_{\rho\sigma}$ resulting from one particular *kth* molecular vibration we substitute equation 7 into 5:

$$\alpha_k = \alpha_0 + \alpha_k^{'} Q_{k_0} \cos(\omega_k t + \delta_k) \tag{8}$$

At this point we bring in the frequency dependence of electric field E written as

$$E = E_0 \cos \omega_1 t \tag{9}$$

And equation 3 becomes

$$p^{(1)} = \alpha_0 E_0 \cos \omega_1 t + \alpha_k^{'} \, E_0 Q_{k_0} \cos(\omega_k t + \delta) \cos \omega_1 t \tag{10}$$

Using the trigonometric function

$$\cos A \cos B = \frac{1}{2} \{\cos(A+B) + \cos(A-B)\} \tag{11}$$

Equation 10 becomes

$$p^{(1)} = \alpha_0 E_0 \cos \omega_1 t + \frac{\alpha_k^{'} E_0}{2} \{\cos(\omega_1 t \pm \omega_k t \pm \delta_k)\} \tag{12}$$

This is the same as

$$p^{(1)} = p_0^{Ray} \cos \omega_1 t + p_0^{Ram} \cos(\omega_1 t \pm \omega_k t \pm \delta_k) \tag{13}$$

Where

$$p_0^{Ray} = \alpha_0 E_0 = \alpha^{Ray} E_0, \text{ and } \quad p_0^{Ram} = \frac{1}{2}\alpha_k^{'} Q_k E_0 \tag{14}$$

It can be clearly seen from the equation 13 that there are three components that correspond to Rayleigh, Stokes Raman and anti-stokes Raman scattering. The $p_0^{Ray} \cos \omega_1 t$ term gives rise to radiation at frequency ω_1 called Rayleigh scattering. The $p_0^{Ram} \cos(\omega_1 + \omega_k)t$ term corresponds

10

to radiation at frequency $(\omega_1 + \omega_k)$ and accounts for anti-Stokes Raman scattering. Finally,

$p_0^{Ram} \cos(\omega_1 - \omega_k)t$ corresponds to radiation at frequency $(\omega_1 - \omega_k)$ and corresponds to Stokes

Raman scattering. [31]

We therefore conclude that classical theory gives a short explanation on scattering of

light of frequency ω_1 incident on a molecule. A harmonically oscillating induced dipole moment

$p^{(1)}$ results from the interaction between the electric field of light and the molecule. The

fluctuation of the induced dipole moment results in the scattering of light at frequencies

$(\omega_1 + \omega_k)$ and $(\omega_1 - \omega_k)$ which correspond to anti-Stokes and Stokes Raman scattering

respectively. We have also seen from equations 1 and 3 that the polarizability is proportional to

the square root of the scattered light intensity. A more detailed treatment of light scattering is

however done using quantum mechanics as shown in the next section.

2.3   QUANTUM MECHANICAL TREATMENT

2.3.1   INTRODUCTION

While classical theory provides the origin of Raman Effect, quantum theory has a more

detailed view. In this treatment, Raman scattering is described by a time dependent perturbation

theory in which an incident electric field perturbs the molecular eigenstates. The induced electric

dipole moment $p^{(1)}$ seen in classical treatment is replaced by a transition electric dipole moment

$(p^{(1)})_{fi}$ associated with a transition in a molecule from initial state i to a final state f that have

been induced by the incident electric field of frequency ω_1. The total induced transition electric

dipole vector is given by the equation:

$$(p)_{fi} = (p^{(1)})_{fi} + (p^{(2)})_{fi} + (p^{(3)})_{fi} + \ldots \tag{15}$$

Where,

$$p^{(1)} = \alpha.E$$
$$p^{(2)} = \frac{1}{2}\beta.EE \tag{16}$$
$$p^{(3)} = \frac{1}{6}\gamma.EEE$$

$p^{(1)}, p^{(2)}, p^{(3)}$ are linear, quadratic and cubic in E respectively. We are therefore, able to obtain

expressions for the first-order induced transition electric dipole moment $(p^{(1)})_{fi}$ and its

corresponding transition polarizability $(\alpha)_{fi}$ as will be seen in equation 22

2.3.2   TIME DEPENDENT PERTURBATION THEORY AND TRANSITION

POLARIZABILITY $(\alpha)_{fi}$

The time dependent Schrödinger equation is given as:

$$H\Psi = i\hbar\,(\frac{d\Psi}{dt}) \tag{17}$$

H is the Hamiltonian operator. Ψ is a time-dependent wave function and can be expressed as a

function of the time-independent wave function by the following equation:

$$\Psi_i^{(0)} = \psi_i \exp(-i\omega_i t) \tag{18}$$

Where ψ_i is the time-independent wave function and $\omega_i t$ is the energy of state i. The perturbed

wave function $\Psi_i{}'$ can be expressed as a linear combination of a series of perturbation terms:

$$\Psi'_i = \Psi_i^{(0)} + \Psi_i^{(1)} + \Psi_i^{(2)} + \dots \tag{19}$$

The total transition electric dipole is thus given by the following operation.

$$(p)_{fi} = <\Psi'_f | \hat{p} | \Psi_i'> \tag{20}$$

From equation 15, the first-order induced transition electric dipole moment is thus obtained by:

$$(p^{(1)})_{fi} = <\Psi_f^{(1)} | \hat{p} | \Psi_i^{(0)} > + <\Psi_f^{(0)} | \hat{p} | \Psi_i^{(1)} > \tag{21}$$

Where $\Psi_i^{(0)}, \Psi_f^{(0)}$ are unperturbed time-dependent wave functions of the initial state i and final f respectively and $\Psi_i^{(1)}, \Psi_f^{(1)}$ are corresponding first-order perturbed time-dependent wave functions. $\hat{p}$ is the electric dipole moment operator. If we assume the virtual states (r) which arise after perturbing a molecule, then obtain a more detailed equation 22. The figure below shows the transition pathway
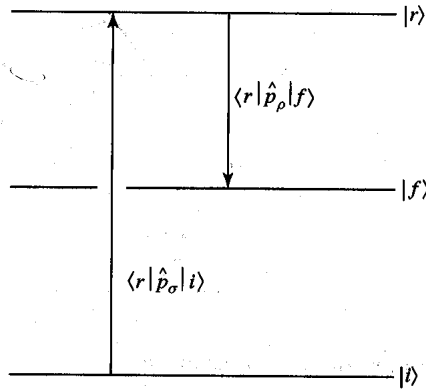
Figure 2. These are linked electric dipole transitions the product of which is shown in equation 22 numerator. $|i>, |f> \: and \: |r>$ are energy levels of the molecule before and after perturbation

We can expand equation 21 by including the time-independent components using equation 18.

$$(p^{(1)}) = (1/2\hbar) \sum_{r \neq i,f} \left\{ \frac{<f|p_\rho|r><\hat{r}|p_\sigma|i>}{\omega_{ri} - \omega_1 - i\Gamma_r} + \frac{<f|p_\sigma|r><r|p_\rho|i>}{\omega_{rf} + \omega_1 + i\Gamma_r} \right\} E_{\sigma 0} \exp{-i\omega_s t} + \text{C.C.} \qquad (22)$$

From equation 16 we can see that the polarizability is a function of the electric dipole moment.

$$(\alpha_{\rho\sigma})_{fi} = (1/\hbar) \sum_{r \neq i,f} \left\{ \frac{<f|p_\rho|r><r|p_\sigma|i>}{\omega_{ri} - \omega_1 - i\Gamma_r} + \frac{<f|p_\sigma|r><r|p_\rho|i>}{\omega_{ri} + \omega_1 - i\Gamma_r} \right\} \qquad (23)$$

In the above equations, the notation has been changed where $|i> \; and < f|$ stand for $|\psi_i> \; and < \psi_f|$ respectively. We have also taken virtual states r into consideration. These virtual states are induced by a perturbation and have lifetimes that relate to Γ_r shown in the denominators of the above equation. The lifetime τ_r is related to $\alpha\Gamma_r$ through the uncertainty principle. Thus $\tau_r = 1/(2\Gamma_r(E))$. In the initial and final states it is assumed that the lifetimes are infinite so that $\Gamma_i = \Gamma_f = 0$.

2.3.3   TYPES OF RAMAN SCATTERING PROCESSES AND

POLARIZABILITY $(\alpha)_{fi}$
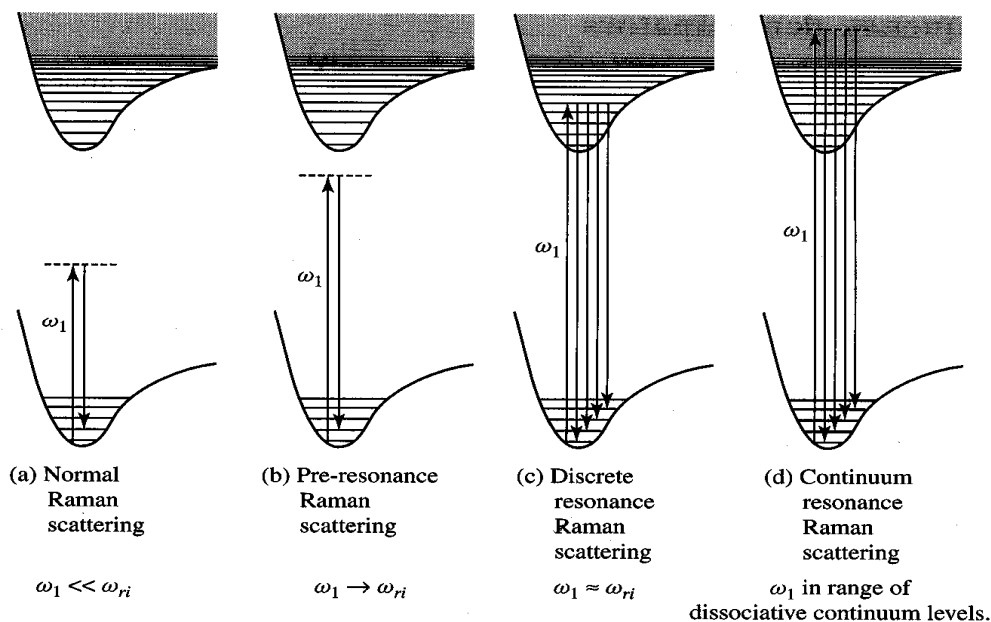
Figure 3. Raman scattering process types as a result of proximity of frequencies $\omega_1 and \omega_{ri}$. Adopted from Long D. A. reference 31

   Four types of scattering processes are described in this section. The polarizability equation 23 is used to describe the rise of the four different scatters. The denominator of this equation ($\omega_{ri} - \omega_1 - i\Gamma_r$) plays a big role in this process. The first instance is where the exciting radiation ω_1 is much smaller than the absorption frequency ω_{ri} (i.e. $\omega_1 << \omega_{ri}$) for all r. This makes $\omega_{ri} - \omega_1 \approx \omega_{ri}$ for all states r and Γ_r can be neglected because they are very small compared to ω_{ri}. This is normal Raman scattering shown in fig 3 (a) and is a result of the molecule interacting with an incident radiation ω_1, making a transition from the initial stationary

state to a so-called virtual state *r* from where it subsequently makes another transition to the final stationary state *f*. The virtual state r is not a solution to the time-independent Schrödinger equation and it doesn't have a well defined value of energy like stationary states *i* and *f* do. The absorption process that involves no energy conservation but gives rise to such virtual states is called virtual absorption.

The frequency ω_1 approaches a molecular transition frequency ω_{ri} and results in what is termed pre-resonance Raman shown in figure 3(b). As $\omega_1 \approx \omega_{ri}$ we get discrete resonance Raman scattering as shown in figure 3(c). If frequency ω_1 is large enough to make the dissociative continuum energy levels of the system the system is called continuum resonance Raman and is illustrated in figure 3(d).

The difference between normal and resonance Raman intensities is a result of how large the excitation frequency ω_1 is compared to the molecular transition frequency ω_{ri} and is explained by the denominator of the above equation. Resonance Raman intensity is usually larger than normal Raman intensity because in the first case the denominator becomes very small when $\omega_1 \approx \omega_{ri}$ (i.e. the denominator is Γ_r dependent) and leads to a larger $(\alpha)_{fi}$ whereas in the second case $\omega_1 << \omega_{ri}$ the denominator is dependent on ω_{ri} (i.e. ω_1 and Γ_r are too small and negligible) hence a smaller $(\alpha)_{fi}$ value. We therefore say that in normal Raman $(\alpha)_{fi}$ is determined by a weighted sum over states $|r>$ of the products $< f | \hat{p}_\rho | r >< r | \hat{p}_\sigma | i >$ and the weighting for each state $|r>$ is inversely proportional to $(\omega_{ri} - \omega_1 - i\Gamma_r)$. Thus normal Raman involves all possible pathways through state $|r>$ that connect the initial state $|i>$ and the final state $|f>$ as seen in figure 2.

The intensity expression is generally written as:

$$I_{fi} = \sigma^R N I_0 W(\Omega) \tag{24}$$

σ^R, N and $W(\Omega)$ represents the total differential cross section ($(cm^2/molc.sr.)$), number of molecules per unit volume and an experimental parameter which is a function of solid collection angle, (Ω).[33] The following equations can be used to calculate the cross section σ^R from intensities obtained from an experiment in which there is a mixture of the sample and an internal standard.

$$\sigma^R = \frac{I_{fi}.\sigma^R(std).c(std).k(std)}{I_{fi}(std).c.k} = \frac{I_{fi}.\sigma^R(std).c(std)}{I_{fi}(std).c} \tag{25}$$

In the above equation c stands for concentration, *std* is the internal standard deviation, and k represents I_0. The cross sections obtained are used to compare the bands from the experimental spectra as will be seen in the experimental section in later chapters of this pamphlet.

3.0   UV-RESONANCE RAMAN STUDY OF THE UNFOLDING BEHAVIOR OF

APOMYOGLOBIN

3.1   **ABSTRACT**

Apomyoglobin is obtained from pure myoglobin by extracting out the heme group. Using
UV-visible spectrometry we are able to monitor complete removal of heme group. This
extraction initiates the disruption of myoglobin's tertiary conformation. Apomyoglobin consists
of 8 α-helices labeled A through H. These helices unfold when the protein is subjected to pH
decrease. It is more compact at about pH 7 and unfolds as we change to more acidic
environment. At about pH 2 we have A, G, H core with the rest of the helices unfolded. At pH
values slightly lower than 2, A, G and H helices are also unfolded. When the protein is not
denatured, the refolding process is done by changing the pH towards neutral. At pH 2, G and H
helices refold and at pH 4 A-helix refolds as well. We have been able to label A-helix with
protons and the rest of the protein with deuterium using H_2O and D_2O respectively. We have
then used temperature change to initiate the unfolding of protonated A-helix. When dissolved in
D_2O, the protonated A-helix at elevated temperatures exchanges its N-H protons to N-D
deuterons. Temperatures were elevated from 0° C to 80°C and changes in Am III peak intensities
were observed using UV resonance Raman spectroscopy. These peak changes were quantified

and used to calculate the number of N-H bonds present between 0° C and 80°C. The number of N-H bonds decreased with increase in temperature indicating the unfolding of A-helix.

3.2   INTRODUCTION

Apomyoglobin (apoMb.) is obtained from myoglobin's single polypeptide chain of helical secondary structures (8 α-helices, labeled A-H) by extracting out the heme group. For protein folding studies, it has been found that heme removal results in the formation of a partially unfolded intermediate. This intermediate structure can be further destabilized with acid denaturation. In recent work, Chi and Asher have used UV resonance Raman (UVRRS) spectroscopy to examine how change in pH of the environment induces changes in secondary structure of apoMb.[34] Resonance Raman involves excitation within the region of the electronic absorption of the peptide bond. In proteins, the amide region is excited by wavelengths 204 nm and 206.5 nm. It is in this range of wavelengths that the amide bonds undergo resonance enhancement in electronic transition from the ground to the excited state.

Using UV resonance Raman spectroscopy it has been possible to determine the existence of three unfolding phases in apoMb (Figure 4).[34] The native state of apoMb (pH 7) was shown to be 62% α-helical. When the functional heme group is removed there is destabilization of the C, D, and F helices (Figure 4, II). At pH 4, a stable AGH intermediate was found to exist, protecting the Trp 14 residues, but with increased water exposure for the Trp 7 residue located on A-helix (figure 4, III). Upon further decrease in pH, the protein further unfolds to only G and H helices (Figure 4, IV).

Based on these studies by Chi and Asher, we have done further research to attempt to label a single helix A and observe how it behaves at different pH values as shown in the next sections of this chapter.
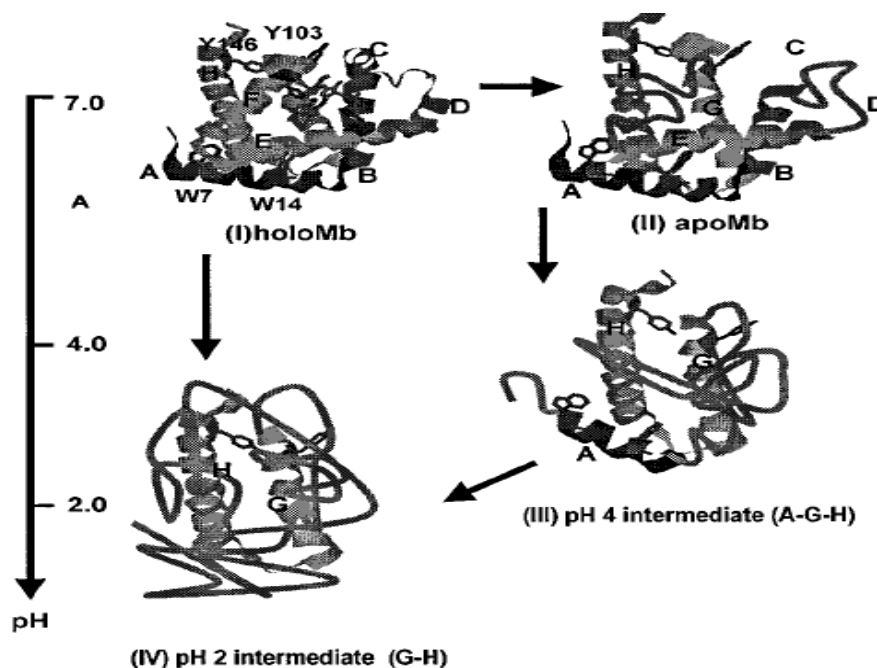
Figure 4. Model for acid denaturation of apoMb and holoMb. The helical structure is represented as ribbons. Lines represent unfolded structures or the so-called β-strands. Adapted from Chi Z. and Asher S.A.[34]

3.3   EXPERIMENTAL

Horse heart myoglobin was obtained from Sigma Aldrich and used as the only source of apomyoglobin (apoMb). Extraction of the heme group was performed using 2-butanone as described in Teale.[35] Absorption spectra in the UV-Vis region were taken to confirm complete removal of the heme group as shown in figure 5.
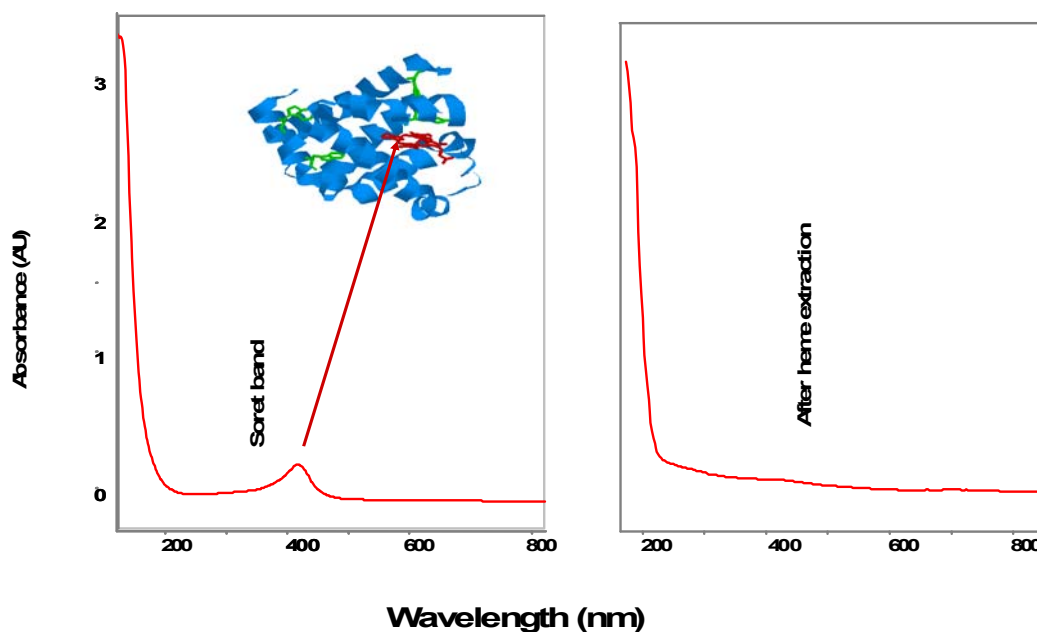
Figure 5. Absorption spectra of myoglobin before and after extraction of heme group. The Soret band at 400 nm disappears which indicates loss of the heme group. Concentration of the original solution was 5 mg/ml.

The freshly made apoMb. was purified using a Waters Delta Prep HPLC with C-18 preparative column. Two detectors at 278 nm and 220 nm were used to detect the protein. The solution containing 50% H_2O, 50% ACN and 0.1% TFA with 20μL of 1 M DTT (Dithiothereitol) was prepared. ApoMb has two Tryptophan chains on the A-helix and were detected after 31 minutes by the both detectors as shown in figure 6. The samples were collected at different times in

21

different bottles corresponding to different peaks and in order to verify which bottle contained

ApoMb, Mass Spectrometer (LC/MS) was used.
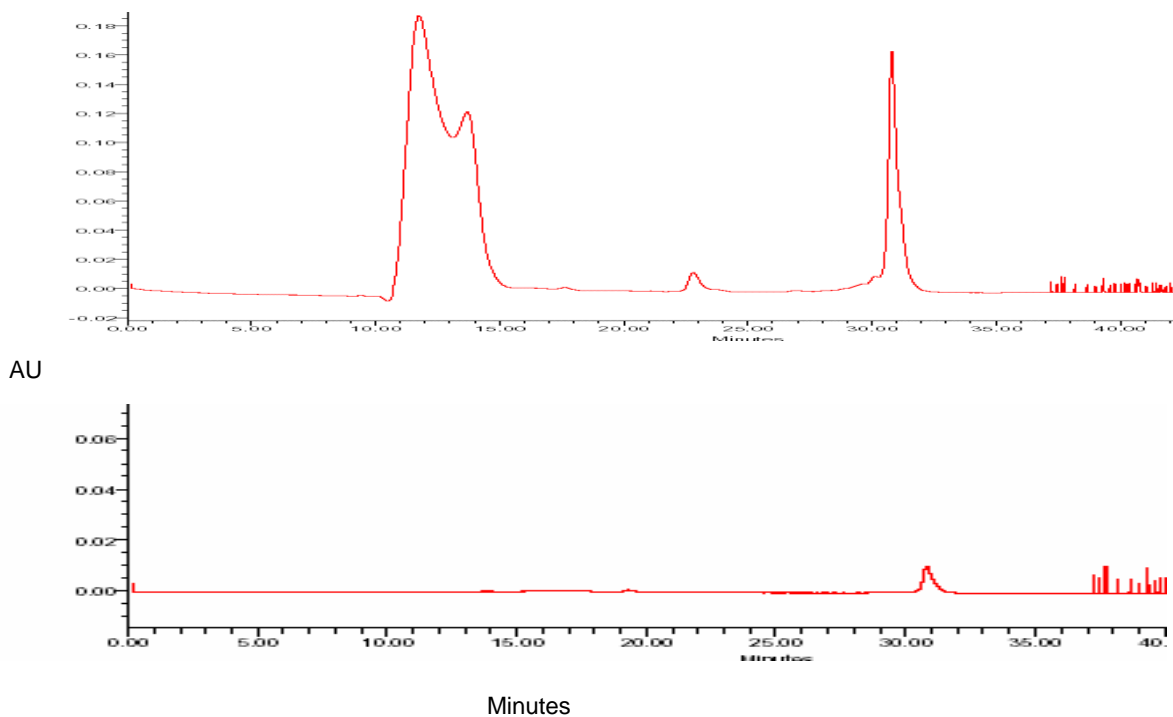
Figure 6. HPLC was used to purify apomyoglobin. The top spectrum is obtained by using 220 nm detector and bottom uses the 278 nm detector. The peak at 31st minute appears in both spectra and corresponds to apomb.

The mass spectrum is shown in figure 7. Six different samples were injected directly into the LC/MS. The apoMb sample was identified using a known apoMb sample. The peak was analyzed as shown in figure 7 and table 1.
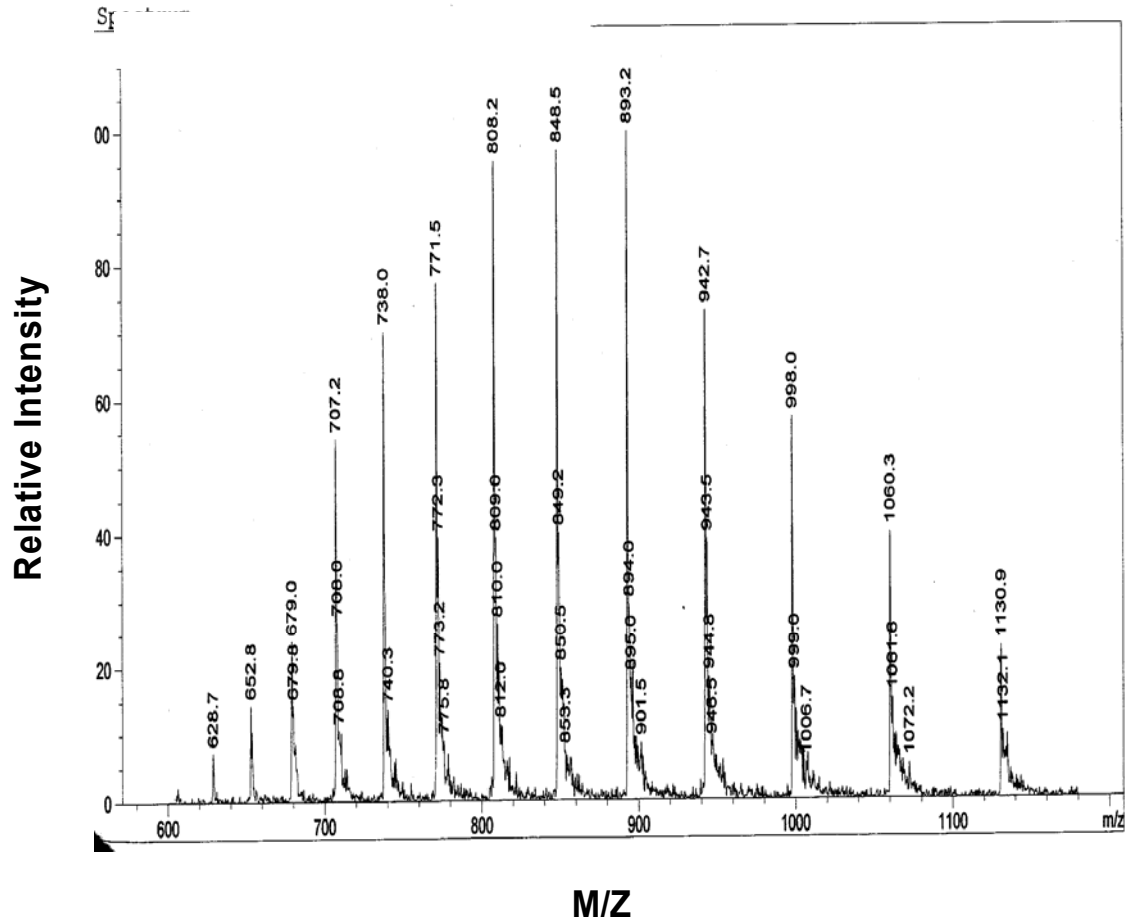
Figure 7. Mass spectrum of Apomyoglobin. The above m/z ratios are indicative of a multi-charged molecule. The charges on this protein are as high as 29+ as shown in a table that follows.

The LC/MS was a true indicator of apoMb presence in the purified sample. The m/z ratios obtained correspond to those of apomyoglobin as calculated in the table 1 below. The calculation uses the molecular weight of horse heart myoglobin.

Z	(M/Z)
14	1211.50
15	1130.80
16	1060.19
17	997.88
18	942.50
19	892.95
20	848.35
21	808.00
22	771.32
23	737.83
24	707.13
25	678.88
26	652.81
27	628.67
28	606.25
29	585.38

- To calculate these charges,
- $m/z = (mw + z*mass) / z$
- Where mw is molecular weight,
- m/z is mass to charge ratio
- z-number of charges
- z* - charge of one proton or sodium depending on which one is attached

Table 1. Calculated charges z obtained from the mass spectrum of apomyoglobin in figure 6. The formula used for this calculation is shown on the table. The molecular weight (mw) of horse heart myoglobin in this case is 16947 g.

The sample was then centrifuged to remove all the organic solvents (mostly acetonitrile). It was then lyophilized for 12 hours to produce powdered apoMb. The new powder was kept at room temperature until needed. For CD experiments, $10 - 20$ μM solutions were prepared. For Raman experiments, about 50 μM solution in D_2O and 60 μM solution in H_2O were prepared.

3.4   RESULTS AND DISCUSSION

A Jasco 715 CD spectropolarimeter was used to study the behavior of apoMb at different pH values at 25 ºC. The sample was dissolved in D_2O and pH adjustments were made using DCl. At pH 2 and lower there was no α-helix observed. We then saw α-helical conformations appear as the pH increased towards neutral as seen in figure 8.
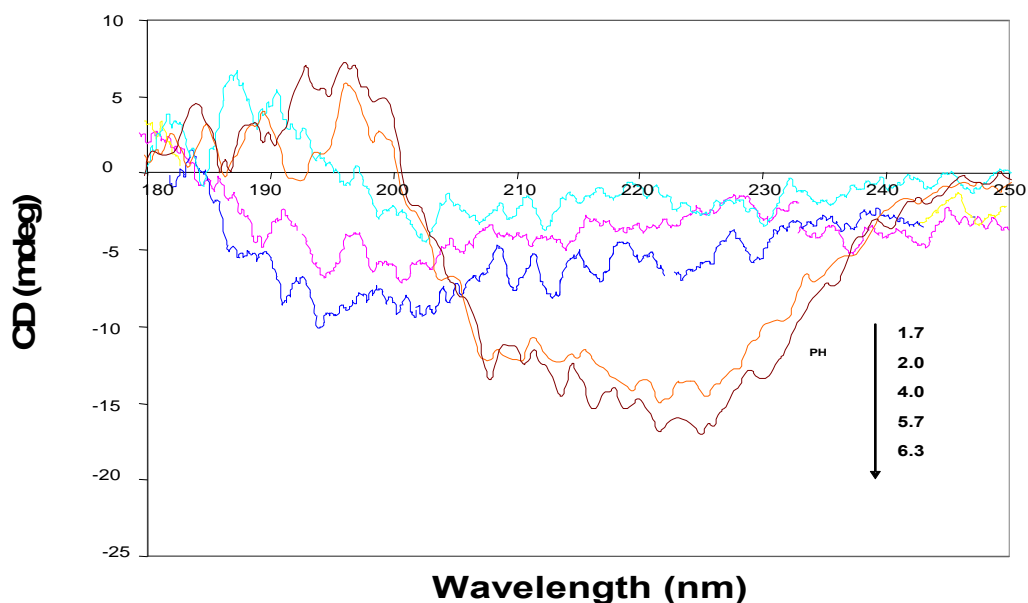
Figure 8. CD spectra of apoMb at different pH values from 1.74 to 6.30. It shows no helical conformation at pH 2 and below. We see α-helix conformation appear at pH 4 and above. Concentrations are about 20 μM ApoMb in D_2O. Temperature was 25º C.

For UV resonance Raman experiments apoMb was incubated in D_2O for 16 hrs at pH 1.74 to deuterate all the helices. ApoMb concentrations of 50 μM in D_2O and 60 μM in H_2O

were used. The goal was to study the behavior of the two solutions at pD 4 and pH 4. Figure 9

shows UV resonance Raman spectra at temperature 10 ºC.
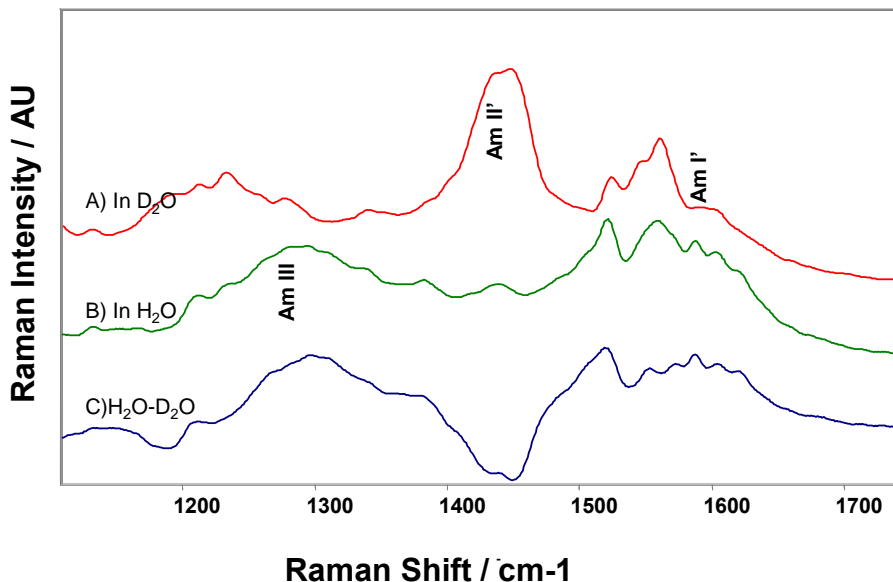
Figure 9. UVRRS excited at 204 nm at 10º C: (A) ApoMb after 16hrs in D$_2$O, pD 4.0.
(B)ApoMb in H$_2$O, pH 4.0. (C) Difference spectra.

From the spectra, we see that the Am II' band in D$_2$O disappears in H$_2$O. We also see the

Am III band in H$_2$O solution disappears in D$_2$O solution because of N-D deuteration. The Am III

band disappears upon N-D deuteration because decoupling between N-H bending and C (O)-N

stretching forms an Am II' band which is almost pure C (O)-N stretching.

The fully deuterated sample (pD <2, incubated in D$_2$O) was brought to pD 2.05 where the

G and H helices refold. It was then frozen in liquid nitrogen and lyophilized. At this point the A-

helix, which is still unfolded was protonated by dissolving the powder in H$_2$O at pH 3.5. The

solution was raised to pH 4 where A-helix refolds with all its N-H protonated. It was frozen and

lyophilized to obtain the solid form with a protonated A-helix. Upon dissolution in D_2O, this sample(A-H) initially contains only protonated peptide bonds in the A-helix.

The solid apoMb with a protonated A-helix was dissolved in D_2O at pD 4.08. This allowed deuterium exchange on the A-helix. The pD 4.08 value was chosen because exchange is slow enough at this pD to prevent complete deprotonation before Raman experiments are performed.[37] Exchange happens due to unfolding of A-helix exposing its N-H bond to D_2O environment. Figure 10. shows 204 nm resonance Raman spectra taken at different temperatures.
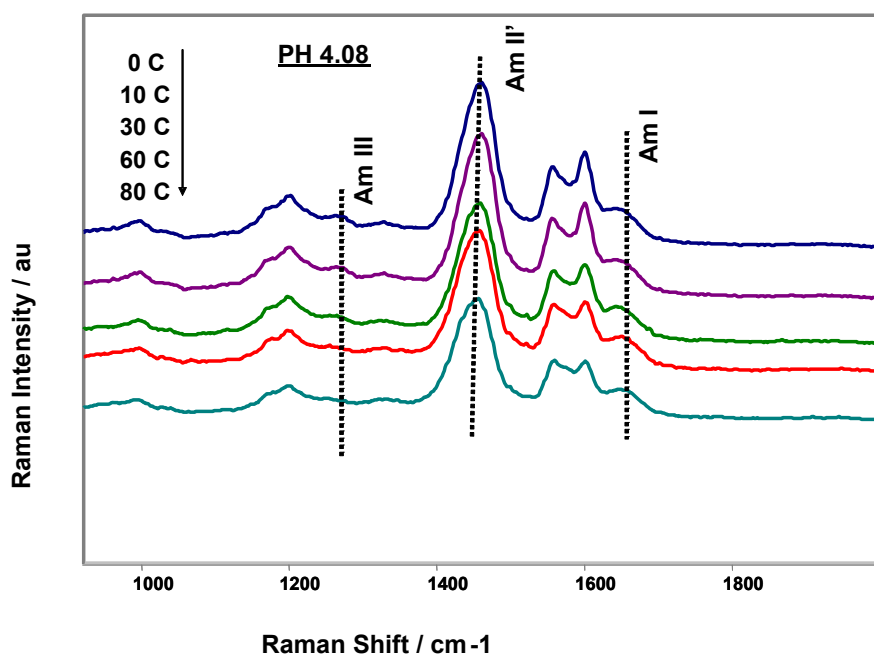
Figure 10. 204 nm UV resonance Raman spectra of apoMb sample measured between 0 and 80 ºC. Three 5 min spectra were recorded and summed. They were normalized with respect to the Am I' band. The change in AmIII region is due to peptide bond deuteration which is facilitated by A-helix melting.

The values of these Fig.10 peak intensities are given in table 2 . The Am III peak vanishes. As the temperature increases the A-helix unfolds and some N-H bonds are exchanged to N-D due to presence of a D_2O environment.
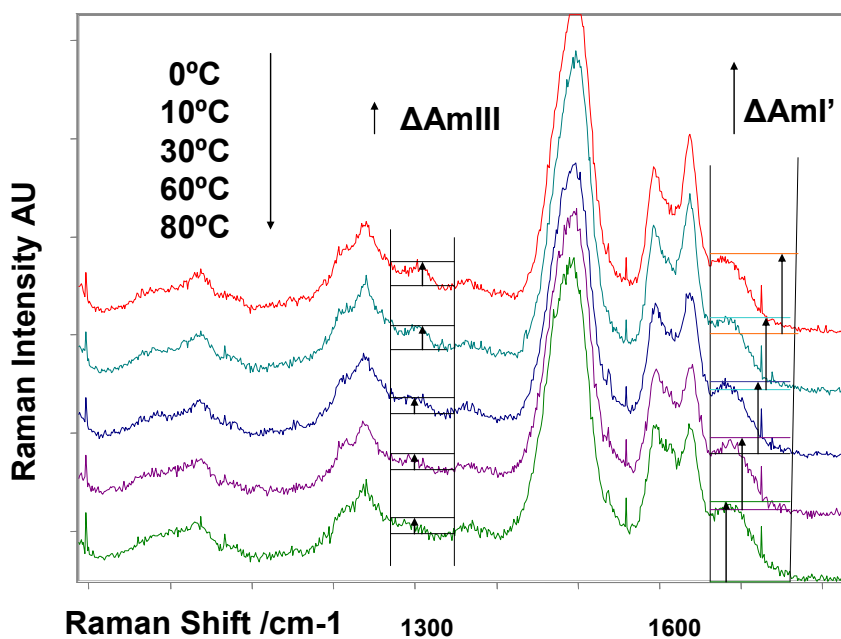
Figure 11. Raman spectra used to estimate peak intensities $I_{AmI'}$ and I_{AmIII} in the Am I' and Am III regions, respectively. Am I' peaks are used to normalize the spectra. The peak intensity results are shown in table 2 below.

Temperature [deg C]	AmI' Intensity /mm	AmIII Intensity /mm	No. of N-H bonds in Am III region
0	20	6.2	62
10	20	6.0	61
30	20	4.5	46
60	20	4.2	43
80	20	4.0	41

Table 2. Table shows Amide I', and III peak heights obtained from figure 11. These intensities $I_{AmI'}$ and $I_{Am III}$, were obtained by normalizing all spectra with respect to Am I' band and using a ruler to measure them as shown in figure 11 above. The last column is obtained using equation 26 (also explained in figure 12).

We can calculate the number of peptide bonds contributing to the Am III region.

$$n_{Am III} = (I_{Am III} \, n_{AmI''} \, \sigma_{AmI'}) / (I_{Am I'} \, \sigma_{AmIII}) \tag{26}$$

Where, $I_{Am III}$ and $I_{Am I'}$ are the integrated intensities of the Am III and Am I' bands, respectively. The number of peptide bonds per protein contributing to the Am III and Am I' band intensities are n_{AmIII} and $n_{AmI'}$, respectively, whereas the $\sigma_{AmI'}$ and σ_{AmIII} are cross sections of the Am I' and Am III bands, respectively.

Assuming equal Am I and Am I' cross sections, we can use the cross sections of the Am I and Am III bands of the α-helical peptides determined by Chi et al.(39) to determine the number of peptide bonds in α-helix like conformations.
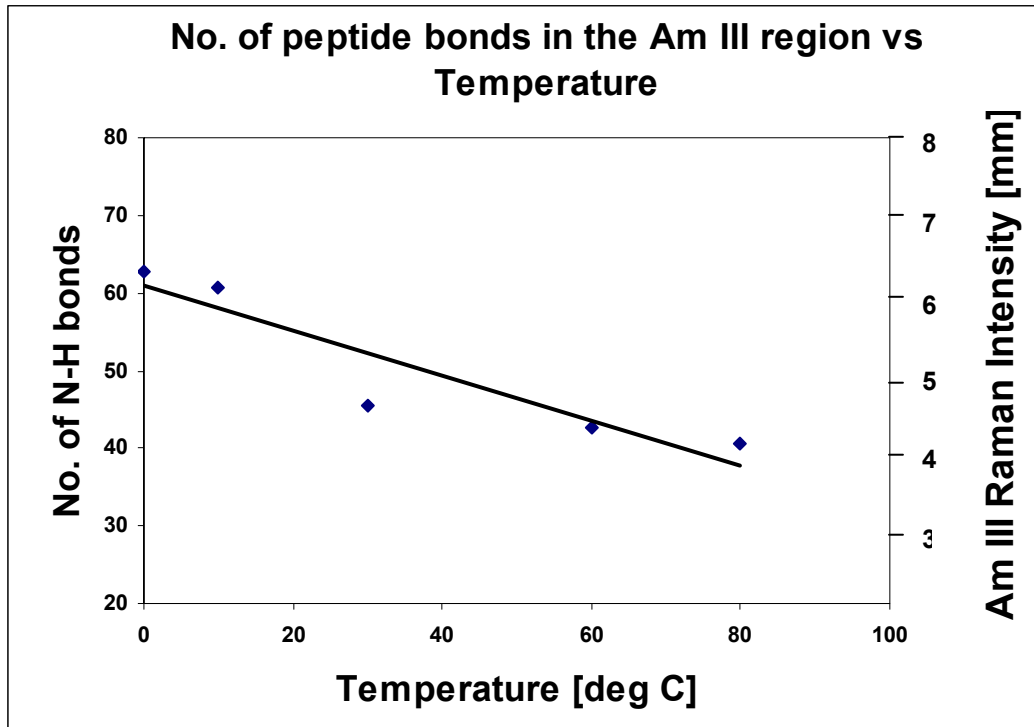
Figure 12. This graph is plotted using data from table 2 which were generated from equation 26. $I_{AmI'}$ and I_{AmIII} were measured in figure 11 and shown in table 2. The number of N-H bonds contributing to Am III band is n_{AmIII} and to Am I' band is $n_{AmI'}$ =152 peptide bonds/protein. The α-helix cross sections are $\sigma_{AmI'}$ =32 mbarn molecule^{-1} sr^{-1} and σ_{AmIII} =24 mbarn molecule^{-1} sr^{-1}, obtained from Chi et al.(39). Also superimposed is the dependence on temperature of Am III intensity normalized with respect to Am I'.

We show in the above figure, that, the number of peptide bonds decreases by approximately 20 peptide bonds between temperatures 0ºC and 80ºC. The observed initial number of peptide bonds is a higher value than the twenty expected from a fully protonated A-helix i.e. 60 peptide bonds at 0 ºC. This could be a result of tryptophan's aromatic band contributing to the AmIII region hence resulting to more intensity than expected. The contribution of tryptophan aromatic band in Am III region is evident from Trpcage study by

Ahmed et al. (1). The loss in number of peptide bonds is approximately twenty which is same number of peptide bonds in the A-helix. We can therefore conclude that this is an evidence of A-helix unfolding.

3.5   CONCLUSION

Preliminary work on this project involved careful extraction and purification of apomyoglobin samples. The methods used included fractional extraction of heme group from horse heart myoglobin using MEK-water mixture and HPLC purification. UV-Vis spectrometry was used to confirm extraction of heme group as seen in figure 5. LCMS was then used to identify apomyoglobin from the purification process. CD spectroctrometry was also used to identify some helical confirmation of apomyoglobin in different pH environment.

The UV resonance Raman experiments were run to study the conformation of A-helix. Experimental results show a decreasing intensity in Am III region as seen in figure 12. We also observed a decreasing number of N-H bonds with increasing temperature same figure. The changes are due to exchange of protonated A-helix with deuterium. It is therefore evident from the above amide band changes that the A-helix can be labeled and can unfold with increase in temperature.

4.0   FUTURE WORK

4.1   TIME RESOLVED MEASUREMENTS OF APOMYOGLOBIN UNFOLDING

T-jump experiment can be done to study the equilibrium conformation of apomyoglobin.
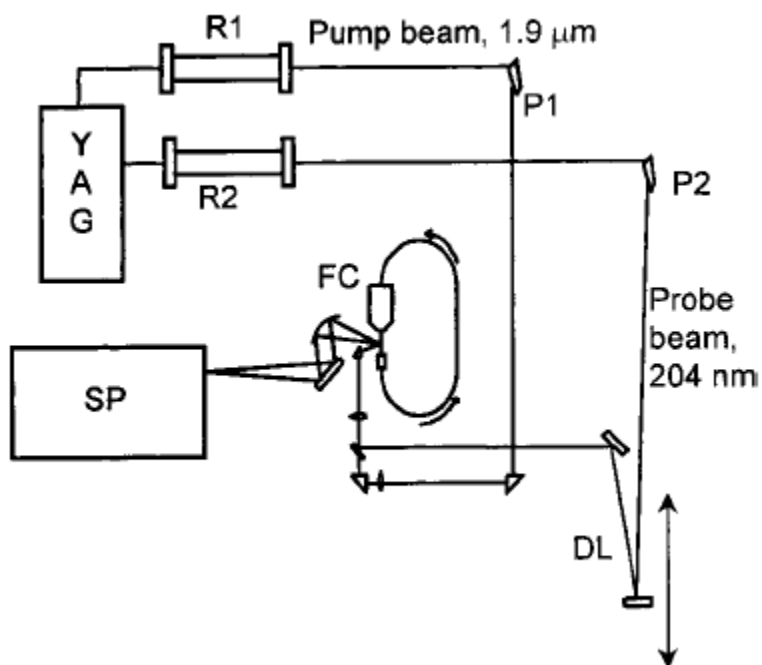The T-jump experimental set-up is described below.

Figure 13. T-jump spectrometer consisting of an Nd: YAG laser, 2 H$_2$ Raman shifters (R1 and
R2), a thermostated flow cell sample circulator (FC) and an ICCD detector (SP).reproduced from
Lednev I. K. reference[38]

There are 2 beams involved in a T-jump experiment, the pump and the probe.[38] The heating pump is acquired by Raman shifting the YAG fundamental in H_2 to 1.9 μm i.e. 1st stokes. The probe beam is obtained by shifting the YAG 3rd harmonic to 204 nm (5th anti-stokes). The time delay between the pump and probe is computer controlled.

The sample is circulated though the two laser beams. The IR heating pump beam is used to heat the solvent (i.e. create a temperature-jump) and the probe is used to detect changes in the protein that the pump beam initiated. We can then take spectra within different time scales (i.e. 3 ns, 5 ns, 10 ns etc) and observe unfolding process.

In future work we would like to do T-jump to study the unfolding kinetics of apomyoglobin. We will prepare apomyoglobin with a labeled A-helix as explained in chapter 3 of this book. We will then initiate unfolding by performing a rapid T-jump with IR pulse as explained in the experimental setup above. A 30 ºC T-jump can be obtained from the sample initially at 35 ºC. This will initiate the A-helix melting. The UVRRS can then be used to examine the unfolding dynamics of protonated A-helix which would show a decreased AmIII integrated peak areas. A concurrent increase of AmII' would be observed. After successfully studying the A-helix, we will use the same methodology on G and H helices.

REFERENCES

1.   Ahmed, Z. UV Resonance Raman spectroscopy of Proteins. Comprehensive thesis
        University of Pittsburgh, Pittsburgh, 2003.

2.   Frank, H. S., Free Volume and Entropy in Condensed Systems I. General Principles.
        Fluctuation Entropy and Free Colume in Some Monatomic Crystals. *Journal of Chemcial
        Physics* **1945,** 13, 478-492.

3.   Frank, H. S., Free Volume and Entropy in Condensed Systems II. Entropy of
        Vaporization in Liquids and the Pictorial Theory of the Liquid State. *Journal of Chemcial
        Physics* **1945,** 13, 493-507.

4.   Frank, H. S.; Evans, M. W., Free Volume and Entropy in Condensed Systems III.
        Entropy in Binary Liquid Mixtures; Partial Molal Entropy in Dilute Solutions; Structure
        and Thermodynamics in Aqueous Electrolytes. *Journal of Chemcial Physics* **1945,** 13,
        507-532.

5.   Asher, S. A.; Chi, Z., UV resonance Raman determination of a-helix melting during the
        acid denaturation of myoglobin. *NATO ASI Series, Series E: Applied Sciences* **1997,** 342,
        (Biomolecular Structure and Dynamics), 263-270.

6.   Asher, S. A.; Chi, Z.; Li, P., Resonance Raman examination of the two lowest amide
        pipi* excited states. *Journal of Raman Spectroscopy* **1998,** 29, (10/11), 927-931.

7.   Asher, S. A.; Ianoul, A.; Mix, G.; Boyden, M. N.; Karnoup, A.; Diem, M.; Schweitzer-Stenner, R., Dihedral ψ angle dependence of the amide III vibration: A uniquely sensitive UV resonance Raman secondary structural probe. *J. Am. Chem. Soc.* **2001,** 123, (47), 11775-11781.

8.   Asher, S. A.; Jones, C. M., UV resonance Raman spectroscopy: a new technique for speciation of aromatics in complex matrixes. *Preprints of Papers - American Chemical Society, Division of Fuel Chemistry* **1986,** 31, (1), 170-80.

9.   Asher, S. A.; Ludwig, M.; Johnson, C. R., UV Resonance Raman excitation profiles of the aromatic amino acids. *Journal of the American Chemical Society* **1986,** 108, (12), 3186-97.

10.   Asher, S. A.; Mikhonin, A. V.; Bykov, S. V., UV Raman Demonstrates that a-helical Polyalanine Peptides Melt to Polyproline II Conformations. *J. Am. Chem. Soc.* **2004,** 126, (27), 8433-8440.

11.   Asher, S. A.; Murtaugh, J. L., UV Raman excitation profiles of imidazole, imidazolium, and water. *Applied Spectroscopy* **1988,** 42, (1), 83-90.

12.   Austin, J. Raman spectroscopic studies of selected enzyme systems. 1989.

13.   Boyden, M. N.; Asher, S. A., UV Raman Studies of Peptide Conformation Demonstrate That Betanova Does Not Cooperatively Unfold. *Biochemistry* **2001,** 40, (45), 13723-13727.

14.   Clore, G. M.; Gronenborn, A. M., NMR of Proteins. **1993**.

15.   Jas, G. S.; Eaton, W. A.; Hofrichter, J., *J. Phys. Chem. B,* **2001,** 105,261-272.

16.   Manas, E. S.; Getahun, Z.; Wright, W. W.; DeGrado, W. F.; Vanderkooi, J. M., Infrared Spectra of Amide Groups in a-Helical Proteins: Evidence for Hydrogen Bonding between Helices and Water. *J. Am. Chem. Soc.* **2000,** 122, (41), 9883-9890.

17.   Ozdemir, A.; Lednev, I. K.; Asher, S. A., Comparison between UV Raman and Circular Dichroism Detection of Short a Helices in Bombolitin III. *Biochemistry* **2002,** 41, (6), 1893-1896.

18.   Kaltashov; A., I.; Eyles; J, S., *Mass Spectrometry Reviews* **2002,** 21, 1893-1896.

19.   Pain, R. H., *Mechanisms of Protein Folding.* ed.; Oxford University Press: New York, NY, 1994; 'Vol.' p.

20.   Ahmed, Z.; Illir, A. B.; Mikhonin, A. V.; Asher, S. A., UV-Resonance Raman Thermal Unfolding Study of Trp-Cage Shows That It Is Not a Simple Two-State Miniprotein. *J. Am. Chem. soc.* **2005,** 127, 10943 -10950.

21.   Neidigh, J. W.; Fesinmeyer, R. M.; Andersen, N. H., Designing a 20-residue protein. *Nature Structural Biology* **2002,** 9, (6), 425-430.

22.   Boyden, M. N. Spectroscopic Investigation of Peptides. University of Pittsburgh, Pittsburgh, 1998.

23.   Asher, S. A., Resonance Raman spectroscopy of hemoglobin. *Methods in Enzymology* **1981,** 76, (Hemoglobins), 371-413.

24.   Asher, S. A., UV Raman Spectroscopy for Analytical, Physical, and Biophysical Chemistry. *Anal. Chem.* **1993,** 65, 59A-66A, 201A-210A.

25.   Myers, A. B., *Chem. Rev.* 96, 3, 911-926.

26.   Lednev, I. K.; Karnoup, A. S.; Sparrow, M. C.; Asher, S. A., Nanosecond UV resonance Raman examination of initial steps in a-helix secondary structure evolution. *Spectroscopy*

of Biological Molecules: New Directions, European Conference on the Spectroscopy of Biological Molecules, 8th, Enschede, Netherlands, Aug. 29-Sept. 2, 1999 **1999**, 11-12.

27.   Creamer, T. P.; Srinivasan, R.; Rose, G. D., Modeling unfolded states of peptides and proteins. *Biochemistry* **1995,** 34, (50), 16245-50.

28.   Creamer, T. P.; Srinivasan, R.; Rose, G. D., Modeling Unfolded States of Proteins and Peptides. II. Backbone Solvent Accessibility. *Biochemistry* **1997,** 36, (10), 2832-2835.

29.   Shi, Z.; Olson, C. A.; Rose, G. D.; Baldwin, R. L.; Kallenbach, N. R., Polyproline II structure in a sequence of seven alanine residues. *Proceedings of the National Academy of Sciences of the United States of America* **2002,** 99, 9190-9195.

30.   Kelly, M. A.; Chellgren, B. W.; Rucker, A. L.; Troutman, J. M.; Fried, M. G.; Miller, A.-F.; Creamer, T. P., Host-Guest Study of Left-Handed Polyproline II Helix Formation. *Biochemistry* **2001,** 40, 14376-14383.

31.   Long, D. A., Raman Spectroscopy. **1977**, 3-84.

32.   Asher, S. A., Ultraviolet Raman Spectroscopy. Handbook of Vibrational Spectroscopy, Vol 1, 2001, John Whiley & Sons, Ltd.

33.   Asher, S. A., *Analytical Chemistry* **1993,** 65(2), 59A-66A.

34.   Chi, Z.; Asher, S. A., Ultraviolet resonance Raman examination of horse apomyoglobin acid unfolding intermediates. *Biochemistry* **1999,** 38, (26), 8196-8203.

35.   Teale, F. W. J., Cleavage of the hemoprotein link by acid methyl ethyl ketone. *Biochim. Biophys. Acta* **1959,** 35, 543.

36.   Asher, S.; Sauer, K., Resonance Raman spectroscopy of manganese(III) etioporphyrin I at the pi -> pi* and charge transfer bands: The use of charge transfer bands to monitor the

complexation state of metalloporphyrins. *Journal of Chemical Physics* **1976,** 64, (10), 4115-25.

37. Englander, S. W., Protein folding intermediates and pathways studied by hydrogen exchange. *Annu. Rev. Biophys. Biomol. Struct.* **2000,** 29, 213-238, 3 Plates.

38. Lednev, I. K.; Karnoup, A. S.; Sparrow, M. C.; Asher, S. A., a-Helix peptide folding and unfolding activation barriers: A nanosecond UV resonance Raman study. *J. Am. Chem. Soc.* **1999,** 121, (35), 8074-8086.

39. Chi, Z.; Chen, X. G.; Holtz, J. S. W.; Asher, s. A.; UV Resonance Raman-Selective Amide Vibrational Enhancement: Quantitative Methodology for Determining Protein Secondary Structure. *Biochemistry* **1998**, 37, 2854-2864